IX SEPOPE
23 a 27 de maio de 2004
May, 23th to 27rd – 2004
Rio de Janeiro (RJ)– Brasil

IX SIMPÓSIO DE ESPECIALISTAS EM PLANEJAMENTO DA OPERAÇÃO E EXPANSÃO ELÉTRICA

IX SYMPOSIUM OF SPECIALISTS IN ELECTRIC OPERATIONAL AND EXPANSION PLANNING

SP–129

ADVANCED TOOL FOR HARMONIC ANALYSIS OF POWER SYSTEMS

Sergio Luis Varricchio
CEPEL

Sergio Gomes Jr.
CEPEL

Nelson Martins
CEPEL

Leandro R. Araujo
FCTJF

Franklin C. Véliz
FCTJF

Cristiano de O. Costa
FCTJF

SUMMARY

The HarmZs program has been developed for the analysis of harmonic problems in power systems. This program makes use of modal analysis that provides additional dynamic information on electrical networks that may be effectively used to improve their harmonic performance. HarmZs also obtains the results produced by the conventional harmonic analysis method, which is based on nodal admittance matrices computed at various discrete values of frequency within the range of interest. This paper describes some aspects and concepts of the conventional and modal analysis of electrical networks as well as highlights some important features of the HarmZs program related to graphical interface and network/equipment modeling.

Keywords: harmonics, modal analysis, descriptor systems, state-space, transfer function, frequency response.

1 INTRODUCTION

The HarmZs program [1] utilizes two recent electrical network-modeling technologies, named Descriptor Systems [2]-[6] and **Y**(*s*) matrix [6]-[12], that allow electrical network analyses over all the complex plane *s* instead of just over the imaginary "*j*ω" axis. The expanded domain of modal analysis provides an important set of dynamic system information that is hard to obtain through use of the two conventional methods: time simulation and frequency response. The information provided by modal analysis includes the natural oscillation modes, identification of equipment that more heavily participate in these modes, modal sensitivities with respect to parameters changes, etc. This additional dynamic information may be effectively used to improve the harmonic performance of electrical networks [3]-[8], [13], [14]. The program also obtains all the results produced by the conventional frequency domain method, which is based on nodal admittance matrices computed at various discrete values of frequency within the range of interest [15]-[18].

Some basic concepts of the conventional and modal analysis methods are reviewed in this paper using a simple electrical system. Details of electrical network and equipment modeling and some features of the graphical interface are also described in the paper.

2 NETWORK MODELING TECHNIQUES SUITABLE FOR MODAL ANALYSIS

The state-space model of electrical networks comprises a set of ordinary first-order differential equations that describe the dynamic behavior of the inductive and capacitive elements [19]. The inductive currents and capacitive voltages constitute the system state variables. The state-space equations describing a linear system (electrical network) can be generically written as:

$$\dot{\mathbf{x}}(t) = \mathbf{A}\,\mathbf{x}(t) + \mathbf{B}\,\mathbf{u}(t) \qquad (1)$$

$$\mathbf{y}(t) = \mathbf{C}\,\mathbf{x}(t) + \mathbf{D}\,\mathbf{u}(t) \qquad (2)$$

where **x** is the state variable vector, $\dot{\mathbf{x}}$ the time derivative of **x**, **u** the input variable vector, **y** the output variable vector, **A**, **B**, **C** and **D** constant matrices, **A** being the system state matrix.

The system states are defined as the minimum set of variables that fully describe the dynamic behavior of the system [19]. Therefore, a minimum set of linearly independent inductive currents and capacitive voltages must be determined. The available techniques to determine this minimum set of states involve an elaborate topological analysis of the electrical circuit which turns the construction of the **A** matrix into a difficult task. These difficulties are eliminated when

using the network-modeling techniques implemented in the HarmZs program, which are explained in the following sub-sections. For the sake of brevity and clarity, only networks having basic RLC components are described. However, more complex components such as long transmission lines [2], [10], [11] and three winding transformers [8] are also properly considered in HarmZs.

2.1 Descriptor System

When modeling electrical networks by the descriptor system technique all inductive currents and all capacitive voltages are assumed to be state variables. It must be pointed out that all methods (eigensolution methods, for example) used in conjunction with the descriptor system model must properly deal with state variable redundancies. Consequently, there are indeed no restrictions in using a set of state variables that is not a minimum set. In addition to the differential and algebraic equations that describe the behavior of each circuit component, the Kirchhoff's current law (KCL) must be written for each circuit node. The KCL equations define the electrical connections among the several circuit elements. In other words, the KCL equations define the network topology.

RLC Series Branch

A RLC series branch connected between the nodes (buses) *k* and *j* is depicted in Figure 1.

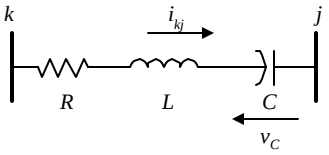

Figure 1: RLC series branch

The dynamic behavior of this element is described by a set of two ordinary differential equations of first order:

$$v_k - v_j = R\, i_{kj} + L\frac{di_{kj}}{dt} + v_C \tag{3}$$

$$C\frac{dv_C}{dt} = i_{kj} \tag{4}$$

where v_k and v_j are the voltages of nodes k and j, respectively. The element variables are the branch current i_{kj} and the capacitor voltage v_C. When there is no capacitor in the branch, (3) and (4) reduce to a single equation:

$$R\, i_{kj} + L\frac{di_{kj}}{dt} = v_k - v_j \tag{5}$$

Note that in the absence of the capacitor, i_{kj} is the only variable in the series branch.

RLC Parallel Branch

A RLC parallel branch connected between the nodes *k* and *j* is depicted in Figure 2.

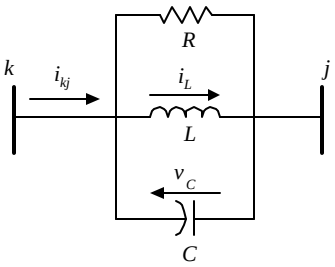

Figure 2: RLC parallel branch

The dynamic behavior of this element is described by:

$$\frac{v_C}{R} + i_L + C\frac{dv_C}{dt} = i_{kj} \tag{6}$$

$$L\frac{di_L}{dt} = v_C \tag{7}$$

$$v_C = v_k - v_j \tag{8}$$

where v_k and v_j are the voltages of nodes k and j, respectively. The element variables are the branch current i_{kj}, the capacitor voltage v_C and the inductive current i_L. When there is no inductor in the branch, (6) and (7) reduce to a single equation:

$$\frac{v_C}{R} + C\frac{dv_C}{dt} = i_{kj} \tag{9}$$

Note that in this case there are two variables, i_{kj} and v_C, in the parallel branch.

The descriptor system modeling may be better explained through an example utilizing the test system pictured in Figure 3.

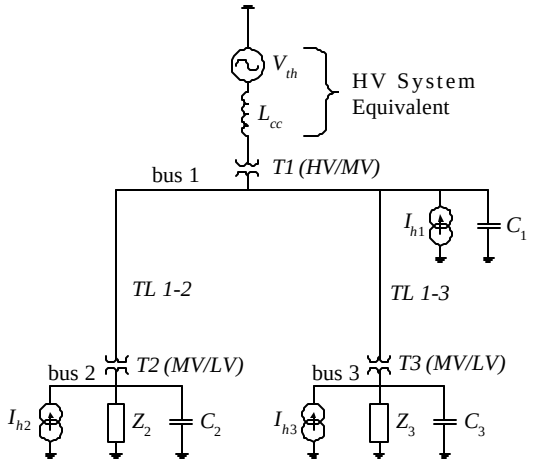

Figure 3: test system

V_{th}: Thévenin voltage. L_{cc}: Short-circuit inductance of the HV system. *T*1: HV/MV transformer. *T*2 and *T*3: MV/LV Transformers. *TL* 1-2: transmission line connecting bus 1 to transformer *T*2. *TL* 1-3: transmission line connecting bus 1 to

transformer *T3*. C_1, C_2, and C_3: capacitor banks connected to buses 1, 2 and 3, respectively. Z_2 and Z_3: load impedances connected to buses 2 and 3, respectively. I_{h1}, I_{h2}, and I_{h3}: harmonic current sources connected to buses 1, 2 and 3, respectively.

This test system can be modeled by the interconnection of several RLC branches as shown in Figure 4.

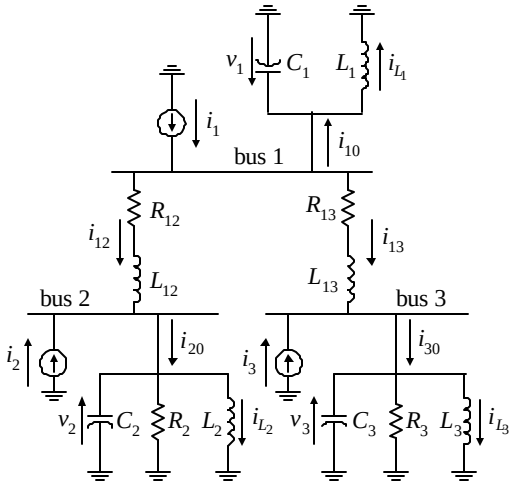

Figure 4: Test system modeling

The symbols L_{12} and R_{12} denote the inductance and resistance of the equivalent series association of the line *TL 1-2* with the transformer *T2*. Similarly, L_{13} and R_{13} represent the inductance a nd resistance of the combined series impedances of the line *TL 1-3* and the transformer *T3*. The impedance loads Z_2 and Z_3 are modeled as shunt reactors (L_2 and L_3) in parallel with shunt resistors (R_2 and R_3).

The descriptor system matrix equations for the test system are shown at the bottom half of this page. These equations are easily assembled when considering the following steps:

1. Apply (6), (7) and (8) to the RLC parallel branches connected between the buses 1, 2 and 3 to ground.
2. Apply (5) to the RLC series branches connected between the buses 1 and 2 and between the buses 1 and 3.
3. Write the KCL for each circuit node (bus).
4. Consider the nodal voltages as output variables and the nodal injected currents as the input variables.

$$
\left[\begin{array}{cccccccccccc|ccc}
L_1 & & & & & & & & & & & & & & \\
 & C_1 & & & & & & & & & & & & & \\
 & & L_2 & & & & & & & & & & & & \\
 & & & C_2 & & & & & & & & & & & \\
 & & & & L_3 & & & & & & & & & & \\
 & & & & & C_3 & & & & & & & & & \\
 & & & & & & L_{12} & & & & & & & & \\
 & & & & & & & L_{13} & & & & & & & \\
\hline
 & & & & & & & & & & & & & & \\
 & & & & & & & & & & & & & & \\
 & & & & & & & & & & & & & &
\end{array}\right]
\frac{d}{dt}
\begin{bmatrix} i_{L_1} \\ v_{C_1} \\ i_{10} \\ i_{L_2} \\ v_{C_2} \\ i_{20} \\ i_{L_3} \\ v_{C_3} \\ i_{30} \\ i_{12} \\ i_{13} \\ \hline v_1 \\ v_2 \\ v_3 \end{bmatrix}
=
\left[\begin{array}{cccccccccccc|ccc}
1 & & & & & & & & & & & & & & \\
-1 & 1 & & & & & & & & & & & & & \\
 & -1 & & & & & & & & & & & 1 & & \\
 & & & 1 & & & & & & & & & & & \\
 & & & -1 & -1/R_2 & 1 & & & & & & & & & \\
 & & & -1 & & & & & & & & & 1 & & \\
 & & & & & & 1 & & & & & & & & \\
 & & & & & & -1 & -1/R_3 & 1 & & & & & & \\
 & & & & & & -1 & & & & & & & 1 & \\
 & & & & & & & & & -R_{12} & & & 1 & -1 & \\
 & & & & & & & & & & -R_{13} & & 1 & & -1 \\
\hline
 & -1 & & & & & & & & -1 & -1 & & & & \\
 & & & & -1 & & & & & 1 & & & & & \\
 & & & & & & & & -1 & & 1 & & & &
\end{array}\right]
\begin{bmatrix} i_{L_1} \\ v_{C_1} \\ i_{10} \\ i_{L_2} \\ v_{C_2} \\ i_{20} \\ i_{L_3} \\ v_{C_3} \\ i_{30} \\ i_{12} \\ i_{13} \\ \hline v_1 \\ v_2 \\ v_3 \end{bmatrix}
+
\left[\begin{array}{ccc}
 & & \\
 & & \\
 & & \\
 & & \\
 & & \\
 & & \\
 & & \\
 & & \\
 & & \\
 & & \\
 & & \\
\hline
1 & & \\
 & 1 & \\
 & & 1
\end{array}\right]
\begin{bmatrix} i_1 \\ i_2 \\ i_3 \end{bmatrix}
\tag{10}
$$

$$
\begin{bmatrix} v_1 \\ v_2 \\ v_3 \end{bmatrix}
=
\left[\begin{array}{cccccccccccc|ccc}
 & & & & & & & & & & & & 1 & & \\
 & & & & & & & & & & & & & 1 & \\
 & & & & & & & & & & & & & & 1
\end{array}\right]
\begin{bmatrix} i_{L_1} \\ v_{C_1} \\ i_{10} \\ i_{L_2} \\ v_{C_2} \\ i_{20} \\ i_{L_3} \\ v_{C_3} \\ i_{30} \\ i_{12} \\ i_{13} \\ \hline v_1 \\ v_2 \\ v_3 \end{bmatrix}
+
\left[\begin{array}{ccc}
 & & \\
 & & \\
 & &
\end{array}\right]
\begin{bmatrix} i_1 \\ i_2 \\ i_3 \end{bmatrix}
\tag{11}
$$

The equations (10) e (11) may be written in a compact form:

$$\mathbf{T}\,\dot{\mathbf{x}}(t) = \mathbf{A}\,\mathbf{x}(t) + \mathbf{B}\,\mathbf{u}(t) \tag{12}$$

$$\mathbf{y}(t) = \mathbf{C}\,\mathbf{x}(t) + \mathbf{D}\,\mathbf{u}(t) \tag{13}$$

When comparing (12) and (13) with (1) and (2), one notes that the state-space and descriptor system formulations differ by the matrix **T**. For the trivial case where **T** equals the identity matrix, the descriptor system degenerates into the state-space formulation.

The electrical network described by (12) and (13) has multiple inputs and multiple outputs. Considering only one input (u) and one output (y), the descriptor system formulation reduces to:

$$\mathbf{T}\,\dot{\mathbf{x}}(t) = \mathbf{A}\,\mathbf{x}(t) + \mathbf{b}\,u(t) \tag{14}$$

$$y(t) = \mathbf{c}^T\mathbf{x}(t) + d\,u(t) \tag{15}$$

The superscript ^{T} denotes matrix or vector transpose. Vector **b** corresponds to one column of matrix **B** and vector $\mathbf{c}^T$ to a row of matrix **C** while d is equal to one element of matrix **D**. Applying the Laplace transform to (14) and (15) yields:

$$s\mathbf{T}\,\mathbf{x}(s) = \mathbf{A}\,\mathbf{x}(s) + \mathbf{b}\,u(s) \tag{16}$$

$$y(s) = \mathbf{c}^T\mathbf{x}(s) + d\,u(s) \tag{17}$$

Solving (16) and (17), and considering $d = 0$, one obtains:

$$y(s) = \mathbf{c}^T(s\,\mathbf{T} - \mathbf{A})^{-1}\mathbf{b}\,u(s) = G(s)\,u(s) \therefore$$

$$G(s) \equiv \mathbf{c}^T(s\,\mathbf{T} - \mathbf{A})^{-1}\mathbf{b} \tag{18}$$

Consider the test system shown in Figure 4 and assume $u = i_2$ and $y = v_3$. The vectors **b** and **c** that define the transfer function $G_{32}(s)$ are then given by:

$$\mathbf{b} = [0\ 0\ 0\ 0\ 0\ 0\ 0\ 0\ 0\ 0\ 0 \,|\, 0\ 1\ 0]^T \tag{19}$$

$$\mathbf{c}^T = [0\ 0\ 0\ 0\ 0\ 0\ 0\ 0\ 0\ 0\ 0 \,|\, 0\ 0\ 1] \tag{20}$$

G_{32} is obtained by substituting (19) and (20) into (18).

2.2 Matrix Y(*s*)

The direct s-domain modeling of the electrical network yields:

$$\mathbf{Y}(s)\,\mathbf{x}(s) = \mathbf{B}\,\mathbf{u}(s) \tag{21}$$

$$\mathbf{y}(s) = \mathbf{C}\,\mathbf{x}(s) + \mathbf{D}\,\mathbf{u}(s) \tag{22}$$

An electrical system comprised of passive elements and driven by current sources, has its **Y**(s) matrix built just as the nodal admittance matrix **Y**($j\omega$) used in the conventional frequency response method. Thus, a diagonal element y_{ii} of the nodal matrix **Y**(s) is calculated as the summation of all elementary admittances connected to node i. Additionally, the off-diagonal elements y_{ij} are equal to the negative value of the summation of all elementary admittances connected between nodes i and j. Replacing the purely imaginary frequency $j\omega$ for the complex frequency s is needed in order to perform modal analysis.

Evaluation of the first derivative of **Y**(s) with respect to the complex frequency s is required when using Newton eigensolution algorithms. This matrix derivative can be analytically obtained following rules similar to those used for building the **Y**(s) matrix.

Consider, for instance, the series and parallel RLC branches shown in Figure 1 and Figure 2. Their admittances are given by the following complex frequency functions:

$$y_{series} = \frac{1}{R + sL + \dfrac{1}{sC}} \tag{23}$$

$$y_{parallel} = \frac{1}{R} + \frac{1}{sL} + sC \tag{24}$$

The derivatives of (23) and (24) with respect to s are given by:

$$\frac{dy_{series}}{ds} = \frac{-L + \dfrac{1}{s^2C}}{\left(R + sL + \dfrac{1}{sC}\right)^2} \tag{25}$$

$$\frac{dy_{parallel}}{ds} = C - \frac{1}{s^2L} \tag{26}$$

The **Y**(s) and $d\mathbf{Y}(s)/ds$ matrices for the test system have the following structure:

$$\mathbf{Y}(s) = \left[\begin{array}{c|c|c} y_{11} & y_{12} & y_{13} \\ \hline y_{21} & y_{22} & 0 \\ \hline y_{31} & 0 & y_{33} \end{array}\right] \tag{27}$$

$$\frac{d\mathbf{Y}(s)}{ds} = \left[\begin{array}{c|c|c} dy_{11}/ds & dy_{12}/ds & dy_{13}/ds \\ \hline dy_{21}/ds & dy_{22}/ds & 0 \\ \hline dy_{31}/ds & 0 & dy_{33}/ds \end{array}\right] \tag{28}$$

The analytical expressions for the diagonal elements y_{11} and dy_{11}/ds are given by:

$$y_{11} = \left(\frac{1}{s\,L_1} + s\,C_1\right) + \left(\frac{1}{R_{12} + s\,L_{12}}\right) + \left(\frac{1}{R_{13} + s\,L_{13}}\right) \tag{29}$$

$$\frac{dy_{11}}{ds} = \left(C_1 - \frac{1}{s^2\,L_1}\right) + \left[\frac{-L_{12}}{(R_{12} + s\,L_{12})^2}\right] + \left[\frac{-L_{13}}{(R_{13} + s\,L_{13})^2}\right] \tag{30}$$

The expressions for the off-diagonal elements $y_{13} = y_{31}$ and $dy_{13}/ds = dy_{31}/ds$ are given by:

$$y_{13} = y_{31} = -\left(\frac{1}{R_{13} + s\,L_{13}}\right) \tag{31}$$

$$\frac{dy_{13}}{ds} = \frac{dy_{31}}{ds} = -\frac{L_{13}}{(R_{13} + s\,L_{13})^2} \tag{32}$$

In the $\mathbf{Y}(s)$ formulation, nodal voltages and currents are related through the equations:

$$\mathbf{Y}(s)\,\mathbf{v}(s) = \mathbf{B}\,\mathbf{i}(s) \tag{33}$$

$$\mathbf{y}(s) = \mathbf{C}\,\mathbf{v}(s) \tag{34}$$

where $\mathbf{v}$ and $\mathbf{i}$ are the vectors for nodal voltages and currents. Comparing (21) and (22) with (33) and (34) one notes that $\mathbf{x}(s) = \mathbf{v}(s)$, $\mathbf{u}(s) = \mathbf{i}(s)$ and $\mathbf{D} = \mathbf{0}$.

When current sources exist in all system buses, matrix $\mathbf{B}$ becomes equal to the identity matrix. Likewise, when the output vector contains all nodal voltages matrix $\mathbf{C}$ becomes equal to the identity matrix. Equations (33) and (34), under these assumptions, reduce to the well-known equations:

$$\mathbf{Y}(s)\,\mathbf{v} = \mathbf{i} \tag{35}$$

$$\mathbf{y} = \mathbf{v} \tag{36}$$

Considering now only one input (u) and one output (y), equations (21) and (22) are reduce to:

$$\mathbf{Y}(s)\,\mathbf{x}(s) = \mathbf{b}\,u(s) \tag{37}$$

$$y(s) = \mathbf{c}^T\mathbf{x}(s) + d\,u(s) \tag{38}$$

Solving (37) for $\mathbf{x}(s)$ and assuming $d = 0$, one obtains after a simple manipulation:

$$y(s) = \mathbf{c}^T\mathbf{Y}(s)^{-1}\mathbf{b}\,u(s) = G(s)\,u(s) \;\therefore$$

$$G(s) \equiv \mathbf{c}^T\mathbf{Y}(s)^{-1}\mathbf{b} \tag{39}$$

Consider again that $u = i_2$ and $y = v_3$ for the test system. The vectors $\mathbf{b}$ and $\mathbf{c}$ that define the transfer function $G_{32}(s)$ are now given by:

$$\mathbf{b} = [0\ 1\ 0]^T \tag{40}$$

$$\mathbf{c}^T = [0\ 0\ 1] \tag{41}$$

3 TRANSFER FUNCTION PLOTTING

The magnitude of transfer function $G_{32}(j\omega)$ is plotted in Figure 5, utilizing the two methodologies available in HarmZs. The red curve is the $|G_{32}(j\omega)|$ frequency response obtained when using the descriptor system model while the blue curve is the same response obtained for the $\mathbf{Y}(s)$ model of the test system. As expected, the two curves are identical.

The test system parameter values are given in Table 1.

Table 1: Test system parameter values

Inductance (mH)		Resistance (Ω)		Capacitance (μF)	
L_{cc}	8.0	R_2	80.0	C_1	23.9
L_2	424.0	R_3	133.0	C_2	8.0
L_3	531.0	R_{12}	0.46	C_3	11.9
L_{12}	9.7	R_{13}	0.55		
L_{13}	11.9				

The HarmZs program allows plotting curves utilizing any of the three visualization tools: the built-in graphical interface, Microsoft Excel or the Plot CEPEL program [20]. In this paper all curves were plotted using Microsoft Excel.

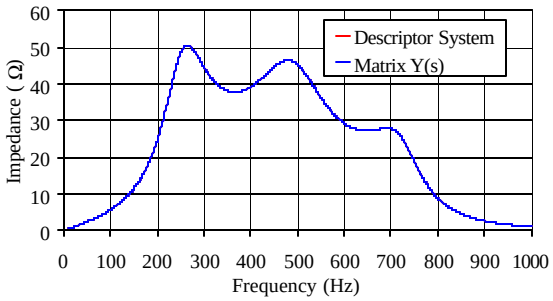

Figure 5: Transfer function $G_{32}(j\omega)$

4 COMPARING THE TWO METHODOLOGIES

The advantages and disadvantages of the Descriptor System and Matrix $\mathbf{Y}(s)$ methodologies are compared [6] in this section.

Descriptor Systems

- ***Main Advantage***

1. The complete set of system poles and transfer function zeros can be simultaneously calculated using the QZ decomposition [21]. These calculations may alternatively be carried out using one-eigenvalue-at-a-time iterative methods (Newton methods) [8]-[11], [22].

- ***Main Disadvantages***

1. Difficulties in modeling frequency dependent parameters.
2. The descriptor system matrices have dimensions that are much larger than the number of system buses.

Matrix Y(s)

- ***Main Advantages***

1. The modeling of frequency dependent parameters is properly accomplished [10], [11].
2. The system matrices have dimension equal or close to the number of system buses. When there are voltages sources to be considered, the dimension is equal to the number of system buses plus the number of voltage sources.

- ***Main Disadvantage***

1. The system poles and the transfer function zeros can only be calculated using one-eigenvalue-at-a-time iterative methods (Newton methods). Powerful eigenvalue deflation techniques, among other strategies rapidly learned by experienced engineers, make practical the use of this modeling technique for large system models.

5 THE IMAGINARY PARTS (FREQUENCIES) OF SYSTEM POLES AND TRANFER FUNCTIONS ZEROS AND THE FREQUENCY RESPONSE PLOT

The relationship between pole and zero frequencies can be summarized as follows [6]:

1. If $s_i = \sigma_i + j\omega_i$ is a system pole or a transfer function $G_{kj}(s)$ zero, then $G_{kj}(\sigma_i + j\omega_i)$ tends to infinity or zero, respectively. However, $G_{kj}(j\omega_i)$ does not approach ∞ or is equal to 0.
2. The $G_{kj}(j\omega_i)$ modulus has a high impedance value (very close to a local maximum) or a low impedance value (very close to a local minimum) depending on whether s_i is a pole or a zero.
3. The frequency ω_i is very close to a parallel or series resonance frequency, depending on whether s_i is a pole or a zero.

The above statements are more easily understood through a test system example. The test system poles and the zeros for the self-impedance (transfer function) of each bus are shown in Table 2.

Table 2: Test system poles and zeros of the bus self-impedances

	Poles	Zeros		
		Bus 1	Bus 2	Bus 3
1	-2.90.08 $\pm j$ 1583.6	-338.52 $\pm j$ 2670.9	-255.47 $\pm j$ 2084.9	-415.26 $\pm j$ 2402.1
2	-507.00 $\pm j$ 3069.1	-804.43 $\pm j$ 3550.6	-93.698 $\pm j$ 3975.6	-398.38 $\pm j$ 4424.9
3	-345.88 $\pm j$ 4535.7	0	0	0
4	-0.98914	-1.0091	-0.99428	-1.0357
5	-1.0419	-1.0549	-26.151	-27.820

The frequencies in Hz (absolute value of the imaginary parts divided by 2π) of the complex conjugate network poles and zeros for the test system (see Table 2) are presented in Table 3.

Table 3: Pole and zero frequencies in Hz

	Poles			Zeros					
				Bus 1		Bus 2		Bus 3	
	1	2	3	1	2	1	2	1	2
f(Hz)	252	488	722	425	565	332	633	382	704

The self-impedance (transfer function) magnitudes as functions of frequency for the three system buses are shown in the next figures. These figures also contain vertical lines connecting the pole and zero frequencies to their respective impedance magnitude values.

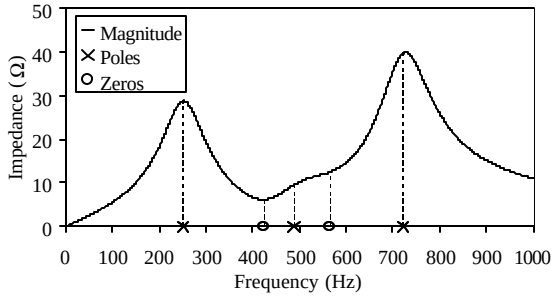

Figure 6: Self-impedance of bus 1

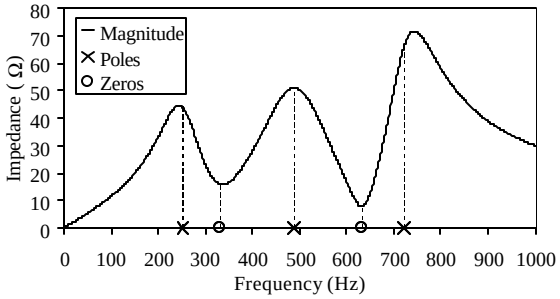

Figure 7: Self-impedance of bus 2

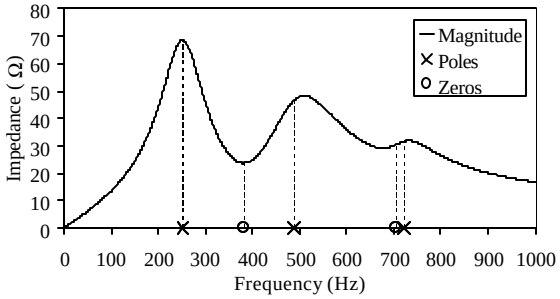

Figure 8: Self-impedance of bus 3

These three figures help explain the pole-zero cancellation phenomenon. For instance, the two zeros of the bus 1 self-impedance (425 Hz and 565 Hz) are close to the pole 2 (488 Hz), having a peak-shaving effect around this frequency value on the magnitude plot of Figure 6. Note also that the second zero of the bus 3 self-impedance (704 Hz) is close to the pole 3 (722 Hz), reducing the impedance magnitude at this frequency as shown in Figure 8.

6 DOMINANT POLES AND REDUCED MODELS

The poles that have the largest associated residue moduli for a chosen transfer function are defined as dominant poles of that transfer function. If these transfer function poles are fairly close to the imaginary axis or, in other words, if they have relatively small real parts, they will produce a high peak in the frequency response magnitude plot.

A transfer function can be written in a partial fraction form:

$$G(s) = \sum_{i=1}^{n} \frac{R_i}{s - \lambda_i} + d \qquad (42)$$

where R_i is the residue associated with the pole λ_i, n is the total number of poles and d is the direct term. Their textbook definitions are [19]:

$$R_i = \lim_{s \to \lambda_i} G(s)(s - \lambda_i) \qquad (43)$$

$$d = \lim_{s \to \infty} G(s) \qquad (44)$$

The HarmZs program does not utilize the above definition of residue in its calculations. There are other equivalent equations, based on eigenvectors, that lead to more efficient computations [9]-[11].

Considering only the dominant poles of the transfer function, the following approximation holds:

$$G(s) \cong \sum_{\Omega} \frac{R_i}{s - \lambda_i} + d \qquad (45)$$

where Ω denotes a chosen set of dominant poles.

The poles and associated residues of the bus 1 and bus 3 self-impedances are shown in Table 4. One should note that complex-conjugate poles have complex-conjugate residues.

Table 4: Poles and associated residues

	Poles	Residue moduli	
		Bus 1	Bus 3
1	-2.90.08 ± *j* 1583.6	8.1782×10^{3}	1.9021×10^{4}
2	-507.00 ± *j* 3069.1	2.5161×10^{3}	2.0353×10^{4}
3	-345.88 ± *j* 4535.7	1.2237×10^{4}	3.3791×10^{3}
4	-0.98914	1.9039×10^{-4}	4.4480×10^{-1}
5	-1.0419	6.5180×10^{-5}	6.2405×10^{-2}

For the bus 1 self-impedance, the pairs of complex conjugate poles 1 and 3 have associated residues with largest moduli, being therefore the most dominant poles for this transfer function. From the magnitude curve of the bus 1 self-impedance (Figure 6), one can indeed verify that these complex-conjugate poles yield the highest peaks. Regarding the bus 3 self-impedance, the pairs of complex conjugate poles 1 and 2 are the most dominants as can be verified in Table 4 or in Figure 8.

Figure 9 and Figure 10 show the self-impedance magnitude plots for bus 1 and bus 3 considering only the two most dominant pairs of complex-conjugate poles (reduced model). Note that the reduced model here is actually a modal equivalent of the specified transfer function. The original plots, considering all poles (complete model), are superimposed for easy comparison. One can see there is good agreement between the corresponding curves.

It must be pointed out that dominant poles and reduced models are very important concepts that help obtaining low order network equivalents of large-scale systems that are used to speed-up engineering studies.

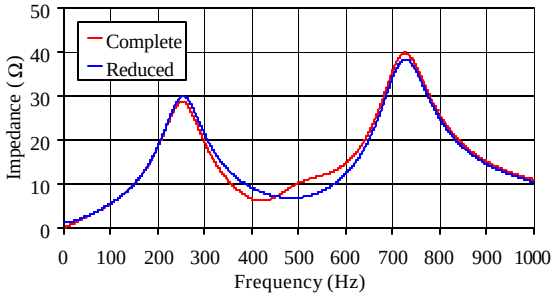

Figure 9: Reduced model of bus 1 self-impedance

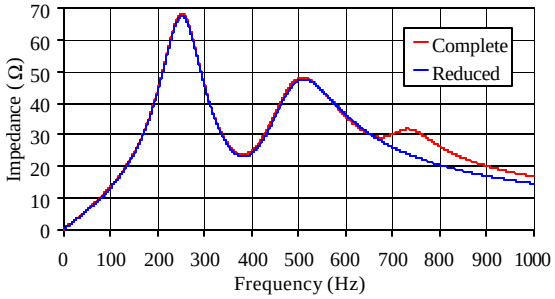

Figure 10: Reduced model of bus 3 self-impedance

7 POLE AND ZERO SENSITIVITIES

The eigenvalue (pole or zero) sensitivity is defined as the rate of change of its real and imaginary parts with respect to a system parameter. Analytical expressions for sensitivity calculation are given in [3], [8], [13], [14]. The sensitivities of the zeros 1 and 2 for the bus 2 self-impedance are given in Table 5.

Table 5: Sensitivities of the zeros of the bus 2 self-impedance $(1 + j \text{ rad})(s^{-1}/\mu F)$

Capacitor	Zero 1	Zero 2
C_1	4.3708 – *j* 9.9007	-4.3708 – *j* 63.708
C_2	0	0
C_3	11.523 – *j* 67.108	15.024 – *j* 37.988

The sensitivities of the zeros 1 and 2 of the bus 2 self-impedance with respect to C_2 are seen, from Table 5, to be null. Therefore, as the value of C_2 is changed the zeros 1 and 2 will remain constant, and so will the series resonances associated with these zeros. The magnitude of the bus 2 self-impedance as a function of frequency is shown in Figure 11 for three values of C_2: 8.0 µF (the original value), 12 µF and 16 µF. As verified in Figure 11, large changes in the value of C_2 practically do not alter the series resonance frequencies.

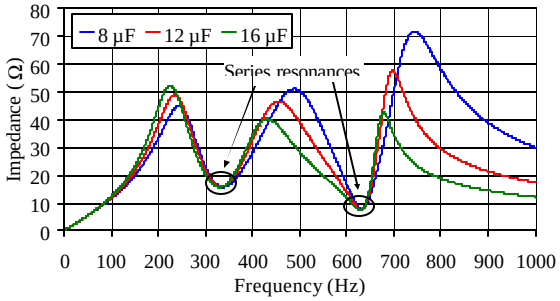

Figure 11: Self-impedance of bus 2 for three values of C_2

8 SHIFTING POLES TO REDUCE HARMONIC DISTORTIONS

This section formulates a harmonic problem for the test system and detailed describes a proposed solution. This solution is based on pole sensitivity information in which the system poles are shifted to more suitable locations in the complex plane in order to reduce harmonic distortions.

8.1 Harmonic Problem Definition

Assume that the bus voltage of the test system (see Figure 4) is 20 kV, the fundamental frequency is 50 Hz and that current sources I_{h1} and I_{h3}, have negligible magnitudes while I_{h2} represents a twelve-pulse converter whose harmonic contents are given in Table 6 in percentage values of the base current. The symbols f, h and I_h denote harmonic frequency, order and contents, respectively. When adopting 10 MVA and 20 kV as base values, the base current turns equal to 288.68 A.

Table 6: Harmonic current components

f(Hz)	550	650	1150	1250	1750	1850
h	11	13	23	25	35	37
I_h (%)	9.09	7.69	4.35	4.00	2.86	2.70

The harmonic voltage at bus 2 is given by the product of its self-impedance magnitude and the injected current modulus, considering each harmonic frequency. On the other hand, the harmonic voltages at buses 1 and 3 are given by the product of the transfer impedance magnitude between them and bus 2 by the injected current modulus. An individual harmonic voltage distortion is expressed as a percentage value of the corresponding phase-to-ground bus voltage.

The self-impedance of bus 2 and the transfer-impedances between buses 1 and 2, and buses 3 and 2 have their magnitudes as functions of frequency presented in Figure 12.

A bar chart showing the individual harmonic distortions at each bus is presented in Figure 13.

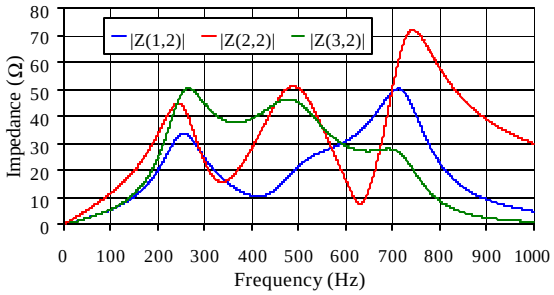

Figure 12: Self-impedance of bus 2 and transfer-impedances between buses 1 and 2, and buses 3 and 2

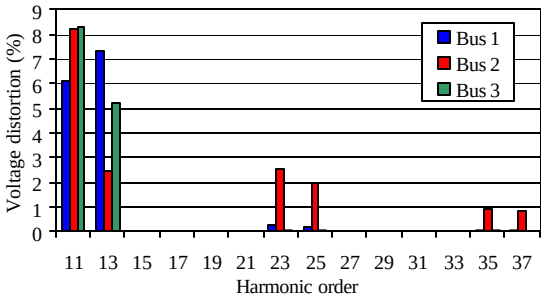

Figure 13: Individual harmonic distortions

8.2 Pole Shifts

The proposed solution for reducing the harmonic voltages distortions consists in shifting the pole 2 (-507.00 + j 3069.1) to the left and the pole 3 (-345.88 + j 4535.7) to the right, by varying the system capacitor values. The first step here considered is the shifting of pole 2. The sensitivities of pole 2 with respect to the three system capacitors are presented in Table 7.

Table 7: Sensitivities of the pole 2 (1 + j rad)(s^{-1}/µF)

Capacitance	Pole 2 (-507.00 + j 3069.1)
C_1	7.1822 – j 3.1098
C_2	13.437 – j 91.449
C_3	18.926 – j 60.418

This table indicates that the pole 2 shifting can be more efficiently accomplished by varying the capacitor C_2. It also indicates that the variation of capacitor C_1 is not effective for the pole 2 shifting. The frequency (imaginary parts divided by 2π) of the pole 2 as a function of changes in the capacitor values at each bus is shown in Figure 14. This figure confirms the sensitivity information given in Table 7. Thus the capacitor at bus 2 was increased by 12 µF in order to bring the frequency of pole 2 to a value smaller than 400 Hz. The system poles for the new C_2 value (20 µF) are presented in Table 8. The original system poles are also presented for easy comparison. The bus 2 self-impedance magnitude and the transfer-impedance magnitude between buses 1 and 2, and buses 3 and 2 as functions of frequency are presented in Figure 15 for C_2 = 20 µF.

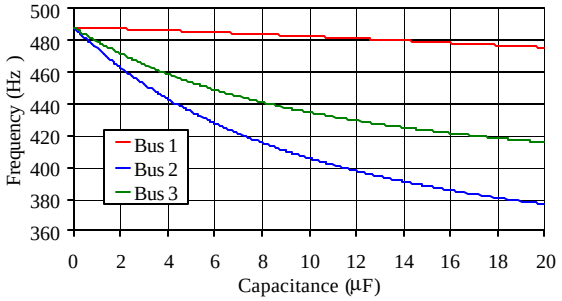

Figure 14: Pole 2 frequency as a function of additional capacitance

Table 8: Comparison between original poles (C_2 = 8 μF) and those obtained for C_2 = 20 μF

Original poles	f (Hz)	Poles for C_2 = 20 μF	f (Hz)
$-290.085 \pm j\ 1583.60$	252.0	$-237.144 \pm j\ 1354.97$	215.7
$-507.008 \pm j\ 3069.12$	488.5	$-331.089 \pm j\ 2499.21$	397.8
$-345.878 \pm j\ 4535.64$	721.9	$-105.987 \pm j\ 4153.33$	661.0
–0.989149	0	–0.989149	0
–1.04187	0	–1.04187	0

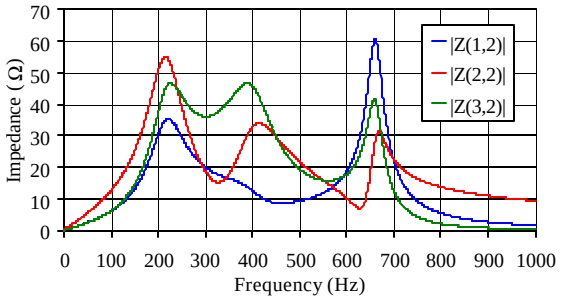

Figure 15: $|Z_{12}|$, $|Z_{22}|$ and $|Z_{32}|$ for C_2 = 20 μF

An undesirable effect produced when increasing the capacitance C_2 was the shifting of pole 3 from 721.9 Hz to 661 Hz. This pole shifting increases the voltage distortions at 13th harmonic (650 Hz). However, the shifting of pole 2 from 488.5 to 397.8 improved significantly the 11th harmonic voltage distortions as seen in Figure 16.

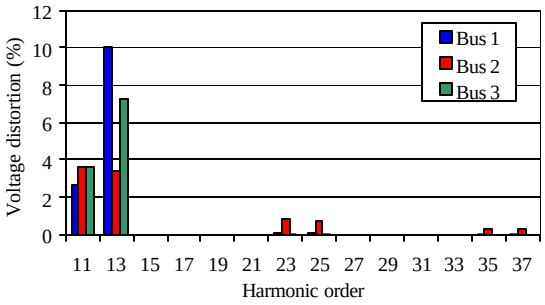

Figure 16: Individual harmonic distortions for C_2 = 20 μF

The shifting to the right of pole 3 (661 Hz) will be pursued next, based on the consideration that C_2 = 20 μF.

The sensitivities of poles 2 and 3 with respect to the system capacitors are presented in Table 9. The frequencies (imaginary parts divided by 2π) of the poles 2 and 3 as functions of a continuous reduction in the capacitance at each bus are plotted in Figure 17 and Figure 18, respectively.

Table 9: Sensitivities of the pole 2 and 3 ($1 + j$ rad)(s^{-1}/μF)

Capacitance	Pole 2 (398 Hz)	Pole 3 (661 Hz)
C_1	$0.27958 - j\ 0.97724$	$-3.5655 - j\ 63.053$
C_2	$7.6650 - j\ 22.906$	$2.9086 - j\ 10.971$
C_3	$12.490 - j\ 62.970$	$9.5310 - j\ 28.445$

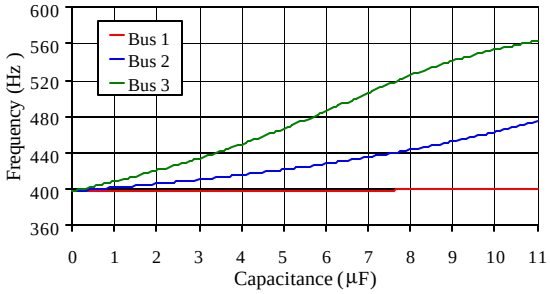

Figure 17: Pole 2 frequency as a function of capacitor reduction at a given bus

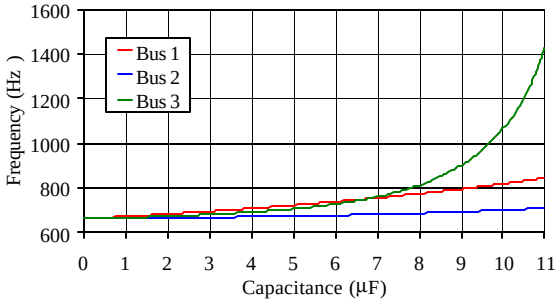

Figure 18: Pole 3 frequency as a function of capacitor reduction at a given bus

Note that the three curves in Figure 17 confirm the sensitivity information given in the second column of Table 9 for the complete range of capacitance variation. On the other hand, Figure 18 confirms the information from the third column of Table 9 just for capacitance changes from 0 to 7 μF approximately. From these results one can see that variations on capacitance C_1 will promote significant shifting in pole 3 practically without any changes in pole 2. Thus the capacitance at bus 1 was decreased by 10 μF in order to make the frequency of pole 3 greater than 800 Hz. The system poles for C_2 = 20 μF and C_1 = 13.9 μF are presented in Table 10. The original system poles are also presented for easy comparison. The self-impedance of bus 2 and the transfer-impedances between buses 1 and 2, and buses 3 and 2 have their magnitudes as functions of frequency presented in Figure 19. The individual harmonic distortions are presented in Figure 20.

Table 10: Comparison between original and for C_2 = 20 µF and C_1 = 13.9 µF poles values

Original poles	f(Hz)	Poles for C_2 = 20 µF and C_1 = 13.9 µF	f(Hz)
–290.085 ± j 1583.60	252.0	–271.788 ± j 1426.71	227.1
–507.008 ± j 3069.12	488.5	–333.847 ± j 2508.85	399.3
–345.878 ± j 4535.64	721.9	–68.586 ± j 5139.13	817.9
–0.989149	0	–0.989150	0
–1.04187	0	–1.04187	0

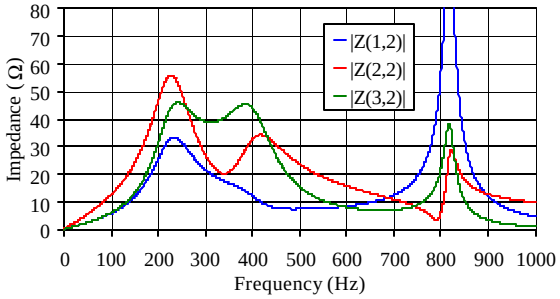

Figure 19: $|Z_{12}|$, $|Z_{22}|$ and $|Z_{32}|$ for C_2 = 20 µF and C_1 = 13.9 µF

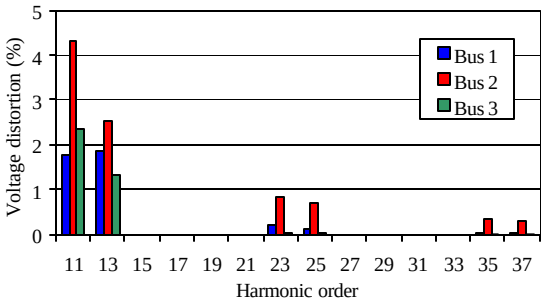

Figure 20: Individual harmonic distortions for C_2 = 20 µF and C_1 = 13.9 µF

Figure 20 shows that the highest distortions occur at bus 2, indicating that the bus 2 self-impedance should be reduced. This may be accomplished by increasing the C_2 value in order to shift the pole 2 (399.3 Hz) to the left once again. It must be pointed out that the zeros of the self-impedance for bus k do not change with the connection of new shunt elements at the same bus k. This is due the fact that the self-impedance becomes null for a s value equal to a zero of this self-impedance. Consequently, the connection of a new shunt element at this bus is short-circuited at this s value and the equivalent impedance remains null. Thus s remains a zero of the bus k self-impedance. This fact was verified in item 7, where the C_2 value was changed and the zeros of bus 2 self-impedance remained exactly the same (see Figure 11). When increasing the value of C_2, the zeros of bus 2 self-impedance do not change while the poles are left-shifted towards their nearest-neighbor zeros. These pole shifts will promote the desired pole-zero cancellation phenomena (seen in item 5) reducing the corresponding peaks in bus 2 self-impedance magnitude curve as shown in Figure 21 for three additional capacitance values. Figure 22 shows the individual harmonic distortions for an additional capacitance value equal to 18 µF (C_2 = 26 µF, which corresponds to the red plot in Figure 21). This is the solution proposed in this paper. The numerical values for the individual harmonic distortions plotted in Figure 13 (original system) and in Figure 22 (proposed solution) are presented in Table 11, as well as the distortions limits [23] adopted in this paper. The symbols used in this table O. S., P. S., h and THD denote original system, proposed solution, harmonic order and total harmonic distortion, respectively.

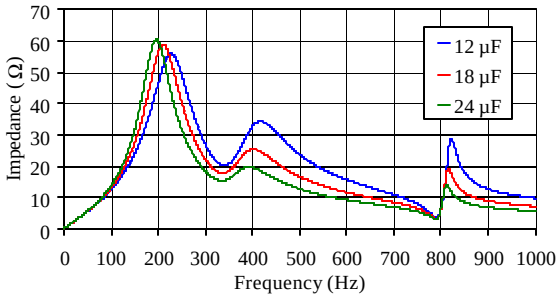

Figure 21: Bus 2 self-impedance for additional capacitance of 12 µF, 18 µF and 24 µF

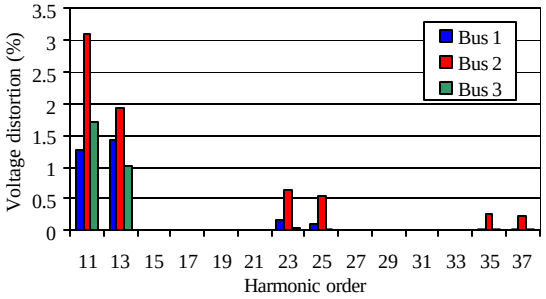

Figure 22: Individual harmonic distortions for C_2 = 26 µF and C_1 = 13.9 µF

Table 11: Harmonic voltages distortions for the original system and proposed solution

	Bus 1		Bus 2		Bus 3		IEC (%)
h	O. S. (%)	P. S. (%)	O. S. (%)	P. S. (%)	O. S. (%)	P. S. (%)	
11	6.14	1.27	8.24	3.12	8.26	1.71	3.50
13	7.30	1.42	2.47	1.92	5.24	1.02	3.00
23	0.279	0.165	2.50	0.639	0.0436	0.0257	1.50
25	0.180	0.102	2.01	0.530	0.0232	0.0132	1.50
35	0.0363	0.0196	0.905	0.259	0.00225	0.00121	1.13
37	0.0283	0.0152	0.798	0.230	0.00156	0.000839	1.08
THD	9.54	1.92	9.26	3.77	9.78	1.99	8.00

9 Conclusions

This paper briefly described some features of the HarmZs program for the analysis of harmonic problems in power systems, as well as some theoretical background needed for understanding the methodologies computationally implemented in the

program. This paper covered a large set of topics, including:

- Network-modeling methodologies suitable for modal and conventional analysis: **Y**(s) matrix and Descriptor Systems. A comparison between these methodologies is presented.
- Transfer function plotting capabilities.
- Calculations and concepts of poles, zeros, their sensitivities to system parameter changes and the pole-zero cancellation phenomenon applied to harmonic analysis.
- Pole residues, dominant poles and reduced models as important concepts to help obtaining low order dynamic network equivalents (modal equivalents) of large scale power systems.
- Formulation of a harmonic problem example using a test system and its effective solution by modal analysis.

10 Bibliography

[1] Sergio Luis Varricchio, Sergio Gomes Jr., Nelson Martins, Leandro Ramos de Araújo and Cristiano de Oliveira Costa, "User Manual of the HarmZs Program V. 1.2", CEPEL Technical Report DPP/POL 1385/02, January 2003 (in Portuguese).

[2] Leonardo T. G. Lima, Nelson Martins and Sandoval Carneiro Jr., "Dynamic Equivalents for Electromagnetic Transient Analysis Including Frequency-Dependent Transmission Line Parameters", *Proceedings of the IPST'97 International Power System Transients* Conference, Seattle, USA, July, 1997.

[3] S. L. Varricchio, N. Martins, L. T. G. Lima and S. Carneiro Jr. "Studying Harmonic Problems Using a Descriptor System Approach", *Proceedings of the IPST'99 - International Conference on Power System Transients*, Budapest, Hungary, June, 1999.

[4] Sergio L. Varricchio and Nelson Martins, "Filter Design Using a Newton-Raphson Method Based on Eigenvalue Sensitivity", *IEEE Proceedings of the Summer Power Meeting*, July 16-20, 2000, Seattle, Washington, USA.

[5] S. L. Varricchio, N. Martins, L. T. G. Lima, "A Newton-Raphson Method Based on Eigenvalue Sensitivities to Improve Harmonic Voltage Performance", *IEEE Transactions on Power Delivery*, vol. 18, no. 1, January 2003, pp. 334-342.

[6] S. L. Varricchio S. Gomes Jr. and N. Martins, "Two Powerful Network Modeling Approaches for the Modal Analysis of Harmonic Problems", *VIII Symposium of Specialists in Electric Operational and Expansion Planning – VIII SEPOPE*, Brasília, Brazil, 19th - 23rd May, 2002.

[7] S. L. Varricchio S. Gomes Jr. and N. Martins, "Modal Analysis of Industrial System Harmonics Using the s Domain Approach", *IEEE Transmission and Distribution Latin America Conference*, São Paulo, SP, Brazil, 18th – 22nd March, 2002.

[8] Sergio L. Varricchio, Sergio Gomes Jr., Nelson Martins "s-Domain Approach to Reduce Harmonic Voltage Distortions Using Sensitivity Analysis", *IEEE Proceedings of the Winter Power Meeting*, Columbus, Ohio, USA, 28 January – 1 February, 2000.

[9] Sergio Gomes Jr., Nelson Martins and Carlos Portela "Modal Analysis Applied to s-Domain Models of ac Networks", *IEEE PES Winter Meeting*, Columbus, Ohio, January 2000.

[10] S. Gomes Jr., C. Portela, N. Martins, "Detailed Model of Long Transmission Lines for Modal Analysis of ac Networks", *Proceedings of the IPST'01 - International Conference on Power System Transients*, Rio de Janeiro, Brazil, June 2001.

[11] Sergio Gomes Jr., Nelson Martins, Sergio Luis Varricchio and Carlos Portela "Modal Analysis of Electromagnetic Transients in ac Networks having Long Transmission Lines", *IEEE Transmission and Distribution Latin America Conference*, São Paulo, SP, Brazil, 18th – 22nd March, 2002.

[12] A. Semlyen, "s-Domain Methodology for Assessing the Small Signal Stability of Complex Systems in Non-Sinusoidal Steady State", *IEEE Transactions on Power Systems*, vol. 6, no. 1, February 1999, pp. 132-137.

[13] Thomas H. Ortmeyer and Khaled Zehar, "Distribution System Harmonic Design", *IEEE Transaction on Power Delivery*, Vol.6, No. 1, January 1991.

[14] J. Martinon, P. Fauquembergue and J. Lachaume, "A State Variable Approach to Harmonic Disturbances in Distribution Networks", *7th International Conference on Harmonics and Quality of Power - 7th ICHQP*, Las Vegas, USA, 16th - 18th October, 1996, pp. 293-299.

[15] G. T. Heydt, "Electric Power Quality", Star in a Circle Publications, 1991.

[16] J. Arrillaga, D. A. Bradley and P. S. Bodger, "Power System Harmonics", John Wiley & Sons, 1985.

[17] R. C. Dugan, M. F. McGranaghan and H. W. Beaty, "Electrical Power Systems Quality", MacGraw-Hill, 1996.

[18] Task Force on Harmonics Modeling and Simulation, "Tutorial on Harmonics Modeling and Simulation", IEEE Special Publication 98TP125-0, 1998.

[19] Thomas Kailath, "Linear System", Prentice-Hall, Inc., Englewood Cliffs, NJ, USA, 1980.

[20] Alex de Castro, Paulo E. M. Quintão, Sergio Gomes Junior, Nelson Martins, Herminio J.C.P. Pinto, "An Integrated Plotting Tool for the Visualization of Results Produced by Multiple Power System Analysis Software", *Proceedings of the IX SEPOPE - Symposium of Specialists in Electric Operational and Expansion Planning*, Rio de Janeiro, RJ, Brazil, May, 23 - 27, 2004

[21] G. H. Golub and C. F. Van Loan, "Matrix Computations", The Johns Hopkins University Press, 1989.

[22] N. Martins, L. T. G Lima and H. J. C. P. Pinto, "Computing Dominant Poles of Power System Transfer Functions", *IEEE Transactions on Power Systems*, vol. 11, no. 1, pp. 162-170.

[23] IEC 1000-3-6-Electromagnetic Compatibility (EMC), Part 3, Section 6: "Assessment of Emission Limits for Distortion Loads in MV and HV Power Systems", First Edition, 1996-10.